# Spatiotemporal Urban Creek Water-Quality Monitoring Using an Open-Source Buoy Style Sensor

Md Asifuzzaman Khan[a], Micah Doberne-Schor[a,b], Sadi Canturk[c], Austin R.J. Downey[a,c], Jasim Imran[c], and Mohammed Baalousha[d]

[a]Department of Mechanical Engineering, University of South Carolina, Columbia, USA
[b]Dreher High School, Columbia, USA
[c]Department of Civil and Environmental Engineering, University of South Carolina, Columbia, USA
[d]Environmental Health Sciences, Arnold School of Public Health, University of South Carolina, Columbia, USA

## ABSTRACT

Conventional water quality monitoring methods that rely on manual sampling and off-site laboratory analysis often fail to provide timely information in dynamic urban water systems. This study presents a spatio-temporal characterization of water quality in an urban creek using a network of buoy-based in situ sensor nodes. Each node integrates sensors for pH, total dissolved solids, turbidity, and temperature. Four nodes were deployed along a one-dimensional transect of the creek, generating time series measurements of these parameters. The resulting dataset was processed using one-dimensional kriging to interpolate water quality parameters between sensor locations over time, producing continuous spatial and temporal profiles. Water quality parameters were monitored before, during, and after a rain event, while water height was recorded using a United States Geological Survey (USGS) stage height data from the creek. Disturbances associated with the rain were then identified by examining changes in the kriged spatio-temporal profiles and by applying Pearson correlation analysis to compare spatial profiles before and after the event. Across the four observation points along the transect, the mean percentage change from before and after the rain event was found to be $-2.87\%$ for pH, $+3.15\%$ for temperature, and $-38.92\%$ for conductivity; while the turbidity data was found to be unreliable due to issues with the selected sensors. These results show distinct, event-associated shifts in the spatial structure of water quality parameters, indicating that natural hydrologic events can introduce measurable changes in water quality distributions in urban streams. Overall, the developed hardware and associated method provide a transferable framework for continuous spatio-temporal monitoring and for assessing event-driven variability in dynamic urban aquatic environments.

**Keywords:** UAV-deployable sensors, water quality, contaminant pulse, kriging, spatio-temporal monitoring, open-source, event-driven variability

## 1. INTRODUCTION

Urban surface waters are highly responsive to short-duration disturbances, and water quality can shift rapidly due to both human activities and natural drivers. While industrial contaminant discharges remain an important concern in urban catchments, a substantial fraction of observed variability in streams and creeks is associated with hydrologic and atmospheric events such as rainfall.[1] Broader natural calamities can also induce measurable water-quality signatures. For instance, wildfires can deposit ash and dissolved ions that increase electrical conductivity[2] when mobilized into waterways.[3] Storms can elevate turbidity through sediment resuspension and watershed runoff,[4] while acid rain can depress pH,[5] altering chemical equilibria and metal solubility. These event-driven responses motivate monitoring strategies that capture rapid transitions and spatial variability.

Further author information: Send correspondence to Austin Downey (austindowney@sc.edu).

Conventional water-quality monitoring commonly relies on manual sampling followed by laboratory analysis, but it is often limited by low sampling frequency, delays in data availability, and sparse spatial coverage. Recent work has demonstrated field-deployable in situ sensing for water-quality monitoring. Osman et al. proposed a low-cost real-time in situ drinking water quality monitoring system using open-source hardware.[6] Hong et al. also proposed a similar system,[7] while Hancock et al. proposed an NMR-based continuous monitoring workflow supported by data-driven analysis.[8] In this work, we present a spatio-temporal monitoring and analysis framework for an urban creek using a network of buoy-based in situ sensor nodes measuring pH, total dissolved solids (or conductivity-derived dissolved-ion content, as applicable), turbidity, and temperature. Four sensor nodes were deployed along a one-dimensional transect to collect synchronized time series. The dataset was processed using one-dimensional kriging[9] to generate continuous spatial profiles and compare pre-event and post-event conditions. A rain event was detected using a United States Geological Survey (USGS) stage height data from the creek, and associated disturbances were characterized using changes in the kriged spatio-temporal profiles and Pearson correlation analysis of spatial profiles before and after the stage increase.

The proposed combination of high-resolution sensing, spatial interpolation, and profile-to-profile similarity analysis is applicable to event detection and attribution in aquatic systems.[10,11] Because many natural calamities produce distinct multi-parameter responses, these measurements can serve as practical indicators of changing watershed conditions, while also supporting the detection of localized anomalies such as short-duration contaminant pulses. The contributions of this work are three-fold: (1) field deployment of a network of open-source, buoy-style in situ sensor networks within an urban creek transect; (2) rain-event segmentation using location-wise Pearson correlation to compare pre- and post-event spatial similarity; and (3) one-dimensional ordinary kriging with uncertainty bounds to produce continuous profiles for spatio-temporal data interpretation.

## 2. METHODOLOGY

This section reports the sensor node's properties, deployment in the creek, and the kriging method.

### 2.1 The Sensor node

The buoy-style sensor node was introduced by Burnett et al.[12] and later refined by Khan et al.[13] The platform used in this study is a variation of this open-source sensor family and includes open-source hardware and software. The design files and firmware are available through a public repository.[14] An overview of the sensor node is shown in Figure 1.

The sensor node weighs 1 kg and measures 34 cm in length. The sensor node is powered by a 3000 mAh lithium polymer battery with a full rated voltage of 12.6 V. When deployed with a full battery, the sensor node lasts about 42 h in continuous operation. The buoy located on the top part of the sensor node helps to keep it upright in water, while the bottom portion with the sensor housing stays submerged. In this study, four sensor

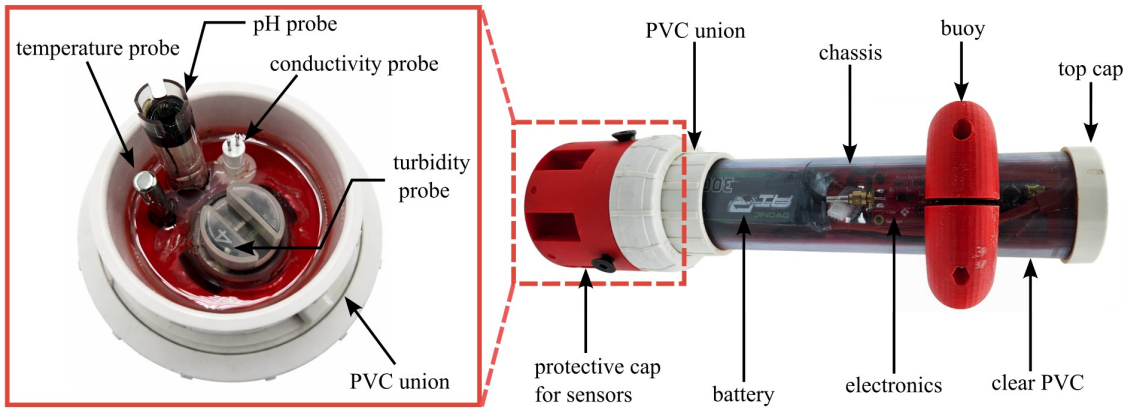


Figure 1. Horizontal view of the fully assembled sensor node. The left inset represents the bottom portion that houses the sensing elements and stays submerged in water.

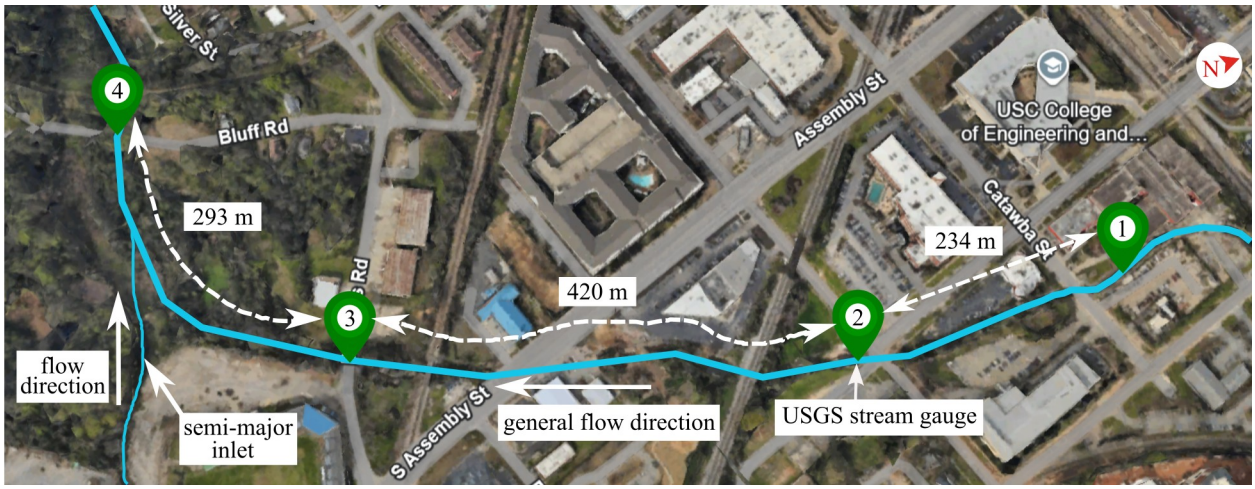


Figure 2. Map view of Rocky Branch creek showing green location markers representing the position of the deployed sensor nodes and the distances between them, starting from number one (upstream) to number four (downstream). Base imagery from Google Earth, © Google; Accessed: Dec 15, 2025.

nodes were deployed in the creek. Measurements of pH, conductivity, and temperature were used for the analysis. Time-series measurements were saved in the onboard microSD card. Turbidity data were not included in the current data assessment due to water intrusion in the turbidity probe of one sensor node during the deployment.

### 2.2 Deployment in creek

Field deployment was conducted in Rocky Branch Creek, an urban stream located in downtown Columbia, South Carolina, that experiences flash flooding.[15,16] Four sensor nodes were installed within the creek, with deployment locations labeled 1 through 4 as shown in Figure 2, with a typical deployment style shown in Figure 3. The inter-node spacing is also indicated in Figure 2, and the overall monitored reach spanned approximately 1 km. There is a semi-major creek inlet to the location of sensor node 4, which is also marked in Figure 2. Sensor node 2 was deployed adjacent to an existing USGS stream gauge station, which provides continuous stage (water height) observations.[17] The stage record from this gauge was used as a hydrologic reference for the deployment period and to identify rain-driven disturbances in the creek. Deployment timing was planned using the local weather forecast to target an anticipated rain event on December 05, 2025; ensuring that the network collected measurements during both pre-rain baseline conditions and a post-rain response period.

### 2.3 One dimensional kriging

To characterize the spatial distribution of water quality parameters along the creek transect, a one-dimensional ordinary kriging[18] (OK) framework is employed. This method provides the best linear unbiased predictor (BLUP)[19] for each measured variable at unsampled locations by accounting for the spatial autocorrelation of the sensor data. For a measured variable $Z$ (such as pH, temperature, or conductivity), the estimated value $\hat{Z}$ at an unsampled location $x_0$ is calculated as a weighted linear combination of the $n$ available observations using.

$$\hat{Z}(x_0) = \sum_{i=1}^{n} \lambda_i z_i, \tag{1}$$

where $z_i$ represents the value observed at location $x_i$, and $\lambda_i$ denotes the kriging weight assigned to the $i$-th observation. In this study, $n = 4$, since 4 sensor nodes are used. To ensure the estimator is unbiased, the summation of the weights are kept equal to 1 ($\sum \lambda_i = 1$). The weights are determined by minimizing the estimation variance, leading to the following system of linear equations,

$$\begin{cases} \sum_{j=1}^{n} \lambda_j \gamma(d_{ij}) + \mu = \gamma(d_{i0}), \quad i = 1, \ldots, n \\ \sum_{i=1}^{n} \lambda_i = 1. \end{cases} \tag{2}$$

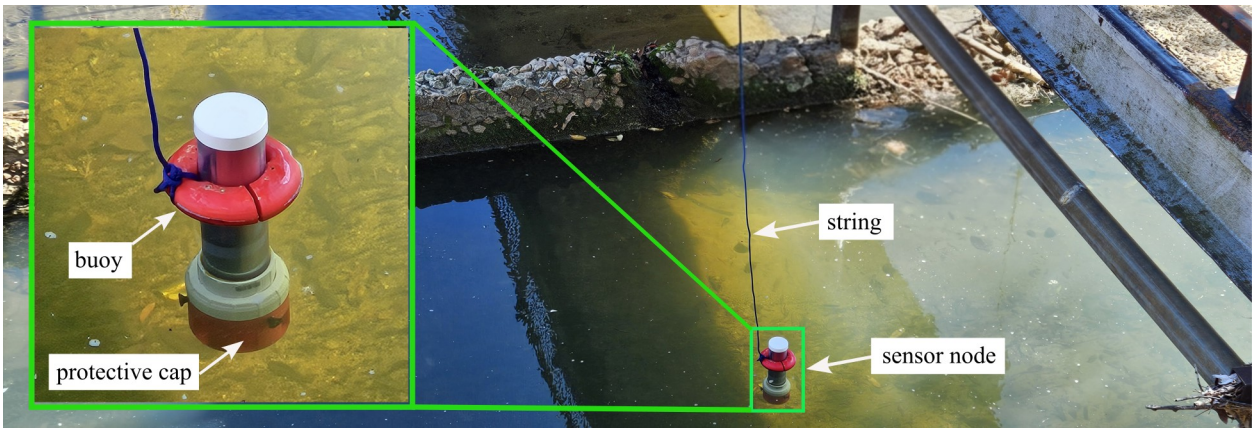


Figure 3. One of the sensor nodes in the creek, tied with a string to hold it in place.

In these equations, $d_{ij}$ is the Euclidean distance between locations $i$ and $j$, $\mu$ is a Lagrange multiplier, and $\gamma(d)$ is the semivariogram model. Given the continuous and smooth nature of the observed water quality gradients, a Gaussian semivariogram model is utilized to describe the spatial dependence using

$$\gamma(d) = c_0 + c\left[1 - \exp\left(-3\frac{d^2}{a^2}\right)\right]. \tag{3}$$

In this model, $c_0$ represents the nugget effect, $c$ is the partial sill, and $a$ denotes the practical range, defined as the distance at which the semivariance reaches 95% of the sill. The uncertainty associated with the spatial estimation is quantified via the kriging variance, defined as

$$\sigma_{\mathrm{K}}^2(x_0) = \sum_{i=1}^{n} \lambda_i \gamma(d_{i0}) + \mu. \tag{4}$$

This variance allows for the derivation of a pointwise 95% confidence interval, expressed as $\hat{Z}(x_0) \pm 1.96\sigma_{\mathrm{K}}(x_0)$, which provides a statistical measure of the interpolation reliability across the studied reach.

## 3. RESULTS

Figure 4 shows the time series data recorded by the four sensor nodes during the creek deployment, which lasted approximately 22 hours. The rain event timing was determined from the USGS stage-height data shown in the bottom plot. The peak stage height of the creek due to rain indicates that the maximum amount of rainwater and associated discharge has accumulated in the creek. The point in time when peak stage height occurred was used as the reference time, and the analysis window was divided into two periods: six hours before the peak stage height and six hours after the peak stage height, as indicated in Figure 4.

The plots show clear differences in the water quality parameters between these two periods. Before the peak stage height (from 0 h to 6 h), pH, temperature, and conductivity remain relatively steady with changes initiating from 4 h as it started raining. After the peak stage height (from 6 h to 12 h), the same parameters exhibit noticeable shifts in magnitude and trend across multiple locations. These contrasting patterns in water quality parameters suggest that the rain event and associated discharge produced measurable changes in water-quality and support the event-based analysis.

Figure 5 shows the location-wise Pearson correlation[20] of pH within the six-hour windows before and after the peak stage height. Before the peak stage height, pH shows moderate to strong positive correlations across the transect, indicating that the four locations followed similar temporal variations under relatively stable flow conditions. After the event, correlations weaken, and some pairs become near-zero or negative, most notably between locations 1 and 4. This change suggests that the rain-driven disturbance introduced spatially non-uniform conditions, such as localized runoff inputs, differences in buffering capacity, or variable mixing along the reach, causing pH to evolve differently at different locations.

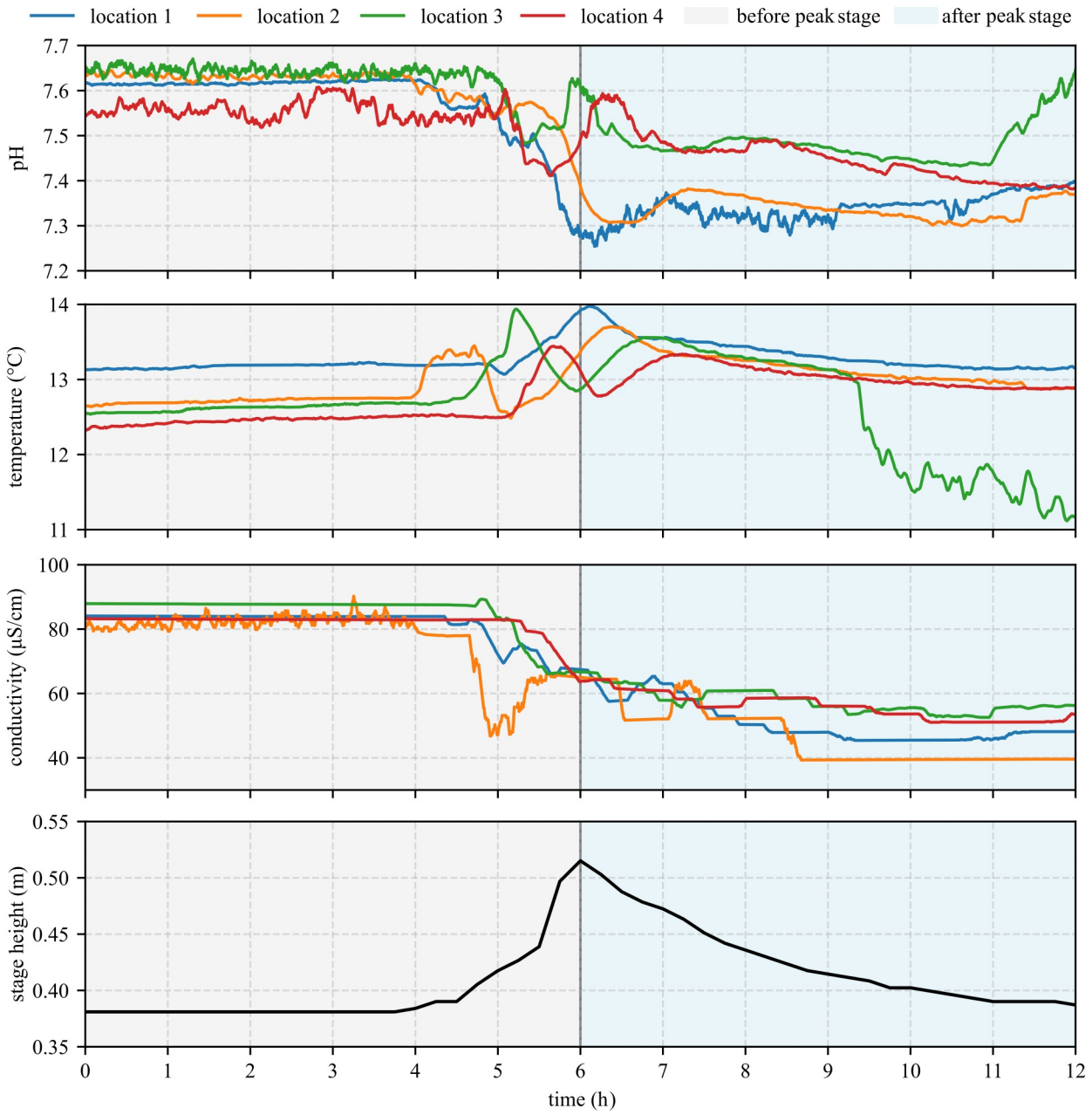


Figure 4. Time series plot of the four sensor node readings from the creek showing pH, temperature, conductivity over four locations, and the water stage height of the creek. The time scale is divided between two regions- 6 hrs before the peak stage height and 6 hrs after the peak stage height, representing before and after rain events.

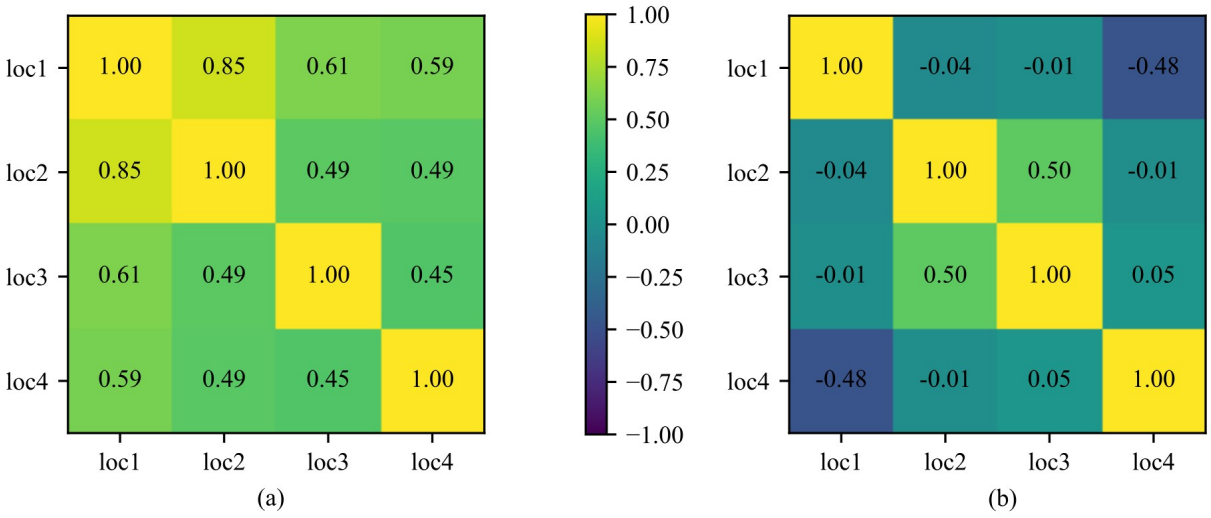


Figure 5. pH location-wise Pearson correlation showing a) before peak stage, and b) after peak stage.

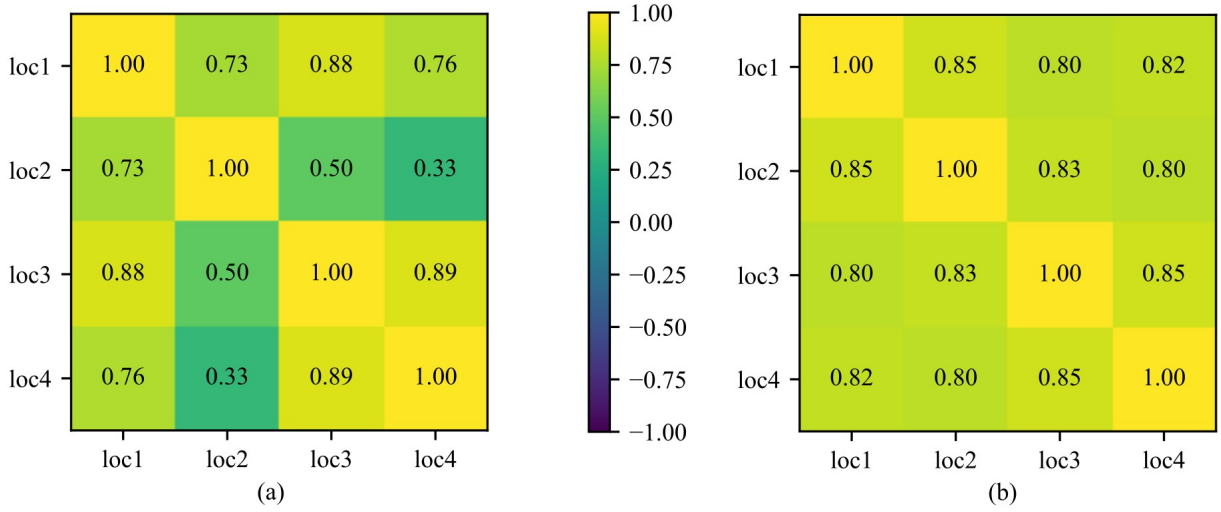


Figure 6. Conductivity location-wise Pearson correlation showing a) before peak stage, and b) peak stage.

Figure 6 reports that conductivity correlations are positive but uneven before the event, with weaker agreement for pairs involving location 2. After the event, correlations increase and become consistently high across all location pairs. A likely explanation is that rainfall increased discharge and promoted along-stream mixing while also producing a broadly similar dilution response across the monitored reach. Under these conditions, conductivity tends to shift more uniformly, which strengthens the similarity among locations.

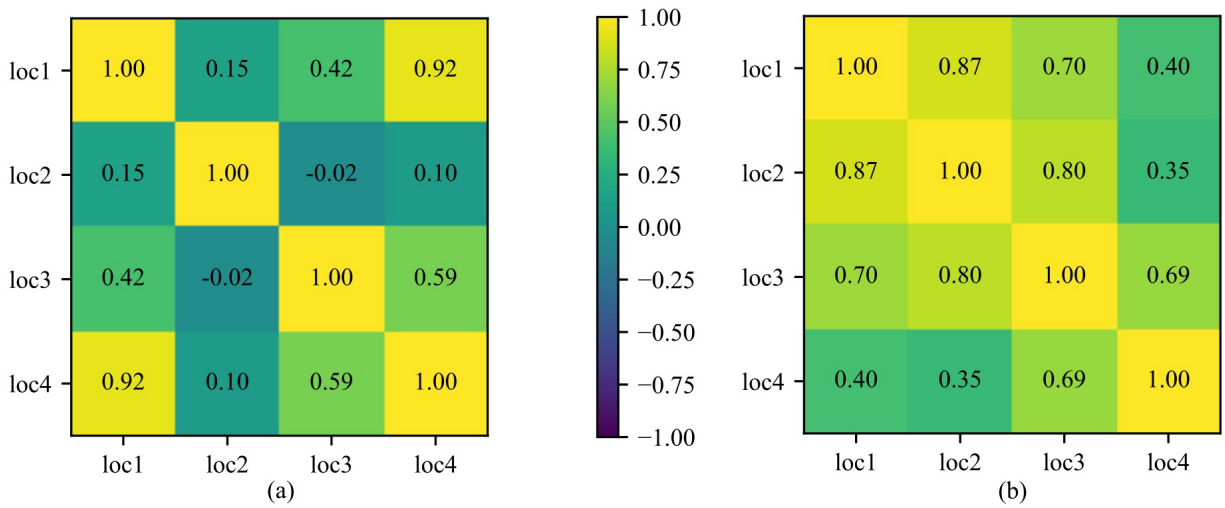


Figure 7. Temperature location-wise Pearson correlation showing a) before peak stage, and b) after peak stage.

Figure 7 shows that temperature exhibits a mixed pattern before the event, including a very strong correlation between locations 1 and 4, while other pairs are weaker. After the event, correlations become stronger among locations 1–3, but remain lower for pairs involving location 4. This behavior is consistent with a rain-driven thermal response that is coherent over part of the reach but modified locally near location 4, potentially due to differences in shading, local inflows, channel geometry, or groundwater contributions that can alter the temperature signal relative to upstream locations.

The correlation results quantify how similarly each parameter varied across the four locations before and after the rain event, but they do not directly represent conditions between sensor sites along the reach. To evaluate the along-stream spatial structure, the one-dimensional kriging approach described in Section 2.3 was applied to interpolate measurements between nodes. Figure 8 shows the resulting profiles for pH, temperature, and conductivity at two representative times, 3 hours before and 3 hours after the peak stage height. The observation markers indicate the sensor readings, and the continuous curves represent the kriging estimates along the transect. The shaded regions denote the 95% confidence bands derived from the kriging variance. In physical terms, these bands represent the range within which the true parameter value is expected to lie with approximately 95% probability under the model assumptions, given the available measurements and the fitted variogram. The bands are narrow near sensor locations, where estimates are strongly constrained by data, and wider between sensors, where uncertainty increases due to interpolation across larger gaps.

To complement the spatial profiles, Table 1 summarizes the relative change in the observed values at each node from 3 hours before to 3 hours after the peak stage height. The table represents both the direction and magnitude of the event-driven response at each observation point and provides the average percentage change across the reach for each parameter. Consistent with the profiles in Figure 8, pH shows an overall decrease, temperature increases downstream, and conductivity exhibits the largest relative reductions, indicating a pronounced shift in ionic strength during the event.

Table 1. Percentage change in water-quality parameters from 3 hrs before to 3 hrs after peak stage height.

| | % change | | | | |
|---|---|---|---|---|---|
| parameter | observation point 1 | observation point 2 | observation point 3 | observation point 4 | average |
| pH | -4.78 | -3.77 | -1.53 | -1.39 | -2.87 |
| temperature | 0.89 | 2.94 | 4.37 | 4.41 | 3.15 |
| conductivity | -41.89 | -51.23 | -33.17 | -29.37 | -38.92 |

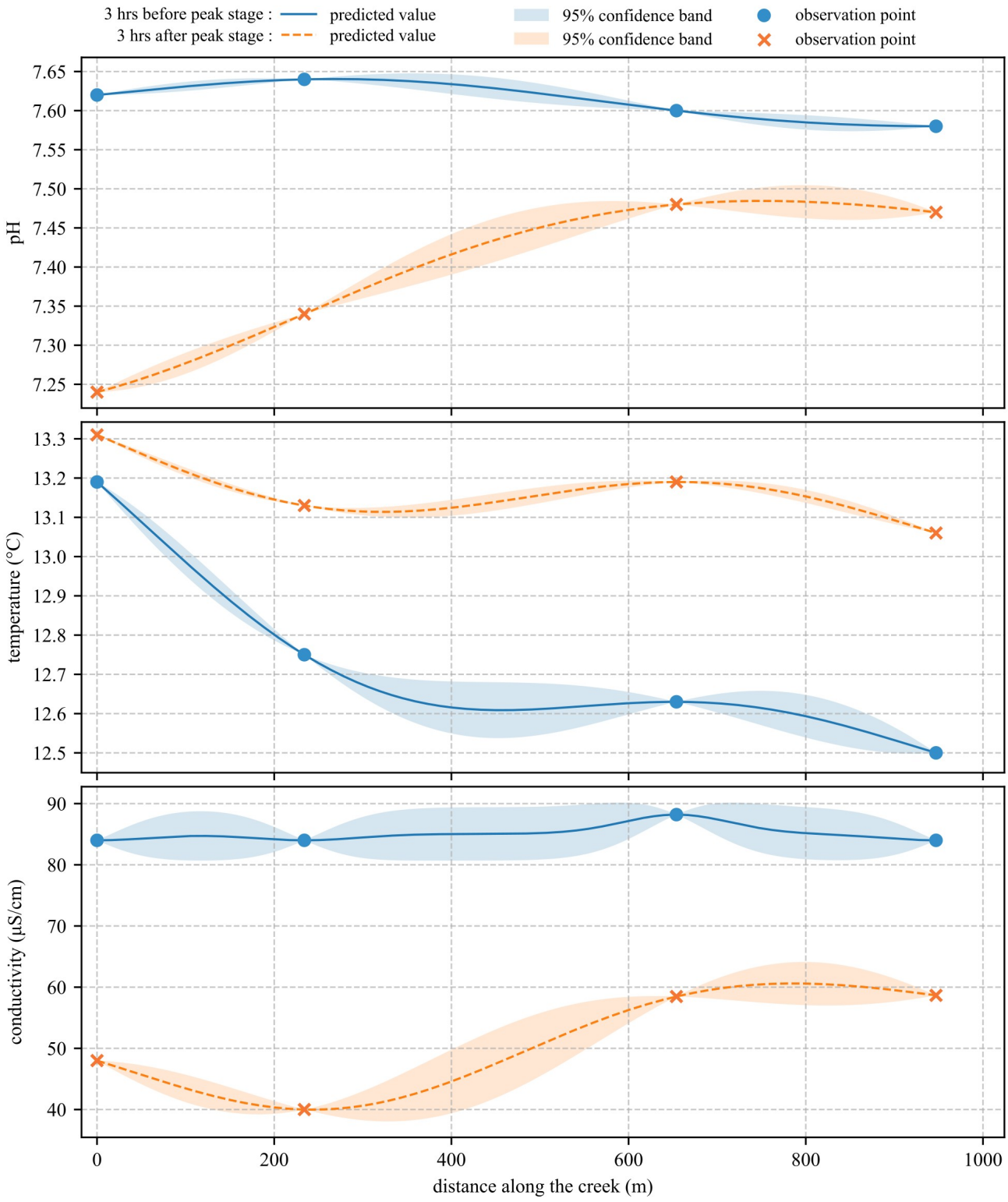


Figure 8. One-dimensional kriging result obtained from the four observation points (four sensors) in the creek.

## 4. CONCLUSION

Event-driven disturbances such as rainfall can rapidly alter urban stream water quality, yet these changes are often missed by conventional sampling due to limited temporal resolution and sparse spatial coverage. Continuous, distributed sensing can improve timely detection and characterization of event-driven water-quality responses and support earlier identification of system changes that are relevant to waterway management, public safety, and downstream infrastructure. The results in this study demonstrate that even a short deployment can capture measurable, reach-scale responses to a rain event and reveal how spatial similarity changes across a creek transect. Across the four observation points in this study, the mean percentage change from before to after the event was $-2.87\%$ for pH, $+3.15\%$ for temperature, and $-38.92\%$ for conductivity. Pearson correlation analysis showed that the rain event altered the spatial coherence of the measurements across the transect. The correlation matrices were computed using the full six-hour window before the peak stage height and the full six-hour window after the peak stage height, providing an overall comparison of pre-event and post-event correlation of each parameter. pH correlations weakened after the event, indicating more spatially heterogeneous behavior, while conductivity correlations increased and became consistently high, consistent with a reach-scale dilution and mixing response. Temperature correlations strengthened among the upstream locations after the event, whereas reduced agreement involving the downstream site suggested localized influences such as shading, tributary inputs, or groundwater exchange. One-dimensional ordinary kriging with a Gaussian variogram model produced continuous along-stream profiles and uncertainty bounds, supporting interpretation of pre- and post-event spatial structure and demonstrating where interpolation uncertainty increased between sensors. In contrast to the correlation analysis, kriging profiles illustrate along-stream spatial variation in a particular point in time (3 h before and after the peak stage height). Overall, the combined use of distributed sensing, correlation-based comparison, and kriging-based interpolation provides a practical and transferable approach for assessing event-driven variability in urban waterways. Future work will include longer deployments across multiple storm events, restoration of turbidity sensing, and evaluation of the framework for detecting shorter-duration anomalies such as contaminant pulses and broader natural hazard signatures.

## ACKNOWLEDGMENTS

This work is supported by the National Science Foundation, United States Grant numbers CMMI - 2152896, CPS - 2237696, and ITE - 2344357. Additional funding for this work comes from the Office of Naval Research through the award number N000142412727, and N000142512404. The support of the National Science Foundation and the Office of Naval Research is gratefully acknowledged. Sadi Canturk is supported by the Ministry of National Education of the Republic of Türkiye through a doctoral scholarship. Any opinions, findings, conclusions, or recommendations expressed in this material are those of the authors and do not necessarily reflect the views of the National Science Foundation, the United States Navy or the Republic of Türkiye.

## REFERENCES

[1] B. Bian, X.-J. Cheng, and L. Li, "Investigation of urban water quality using simulated rainfall in a medium size city of China," *Environmental Monitoring and Assessment* **183**, pp. 217–229, Mar. 2011.

[2] J. S. Martin, A. R. J. Downey, M. Baalousha, and S. H. Won, "Rapid measurement of magnetic particle concentrations in wildland–urban interface fire ashes and runoff using compact NMR," *IEEE Sensors Journal* **24**, pp. 7355–7363, Mar. 2024.

[3] M. J. Paul, S. D. LeDuc, M. G. Lassiter, L. C. Moorhead, P. D. Noyes, and S. G. Leibowitz, "Wildfire induces changes in receiving waters: A review with considerations for water quality management," *Water Resources Research* **58**, Sept. 2022.

[4] R. Mukundan, D. Pierson, E. Schneiderman, D. O'Donnell, S. Pradhanang, M. Zion, and A. Matonse, "Factors affecting storm event turbidity in a New York City water supply stream," *CATENA* **107**, pp. 80–88, Aug. 2013.

[5] P. Middleton and S. L. Rhodes, "Acid rain and drinking water degradation," *Environmental Monitoring and Assessment* **4**, pp. 99–103, Mar. 1984.

[6] S. O. Osman, M. Z. Mohamed, A. M. Suliman, and A. A. Mohammed, "Design and implementation of a low-cost real-time in-situ drinking water quality monitoring system using arduino," in *2018 International Conference on Computer, Control, Electrical, and Electronics Engineering (ICCCEEE)*, pp. 1–7, IEEE, Aug. 2018.

[7] W. Hong, N. Shamsuddin, E. Abas, R. Apong, Z. Masri, H. Suhaimi, S. Gödeke, and M. Noh, "Water quality monitoring with arduino based sensors," *Environments* **8**, p. 6, Jan. 2021.

[8] D. Hancock, D. P. Wamai, M. A. Khan, W. Janvrin, A. R. J. Downey, M. Baalousha, and T. M. Crawford, "Continuous water quality monitoring using field deployable NMR and explainable AI," in *Ocean Sensing and Monitoring XVII*, W. Hou, L. J. Mullen, and J. Jackson, eds., p. 15, SPIE, May 2025.

[9] Y.-C. Chen, H.-C. Yeh, and C. Wei, "Estimation of river pollution index in a tidal stream using kriging analysis," *International Journal of Environmental Research and Public Health* **9**, pp. 3085–3100, Aug. 2012.

[10] J. E. Quansah, B. Engel, and G. L. Rochon, "Early warning systems: A review," *Journal of Terrestrial Observation* **2**(2), p. 5, 2010.

[11] C. A. Emmerton, C. A. Cooke, S. Hustins, U. Silins, M. B. Emelko, T. Lewis, M. K. Kruk, N. Taube, D. Zhu, B. Jackson, M. Stone, J. G. Kerr, and J. F. Orwin, "Severe western Canadian wildfire affects water quality even at large basin scales," *Water Research* **183**, p. 116071, Sept. 2020.

[12] M. Burnett, M. Abdelwahab, J. N. Satme, A. R. J. Downey, G. Barahona Smith, A. Fonce, and J. Imran, "UAV-deployable open-source sensor nodes for spatial and temporal in situ water quality monitoring and mapping," *Sensors* **26**, p. 1158, Feb. 2026.

[13] M. A. Khan, M. Burnett, A. R. J. Downey, J. N. Satme, and J. Imran, "UAV deployable buoy-style sensor for in situ water quality monitoring," in *Ocean Sensing and Monitoring XVII*, W. Hou, L. J. Mullen, and J. Jackson, eds., p. 14, SPIE, May 2025.

[14] ARTS Laboratory, "In-situ water-quality sensor." https://github.com/ARTS-Laboratory/In-Situ-Water-Quality-Sensor/tree/main/System_development/Jocassee/V0.5.1.

[15] A. H. Tanim, C. Smith-Lewis, A. R. Downey, J. Imran, and E. Goharian, "Bayes_opt-swmm: A Gaussian process-based Bayesian optimization tool for real-time flood modeling with SWMM," *Environmental Modelling and Software* **179**, p. 106122, Aug. 2024.

[16] S. Shin, S. Lee, D. Judi, M. Parvania, E. Goharian, T. McPherson, and S. Burian, "A systematic review of quantitative resilience measures for water infrastructure systems," *Water* **10**, p. 164, Feb. 2018.

[17] U.S. Geological Survey, "Rocky Branch at Whaley St at Columbia, SC (USGS-02169506) — USGS water data for the nation." https://waterdata.usgs.gov/monitoring-location/USGS-02169506/#dataTypeId=continuous-00065-0&period=P7D&showFieldMeasurements=true. Accessed: 2025-12-04.

[18] A. Papritz and A. Stein, *Spatial prediction by linear kriging*, pp. 83–113. Springer Netherlands, 1999.

[19] O. Berke, "Estimation and prediction in the spatial linear model," *Water, Air, and Soil Pollution* **110**, pp. 215–237, Mar. 1999.

[20] J. Benesty, J. Chen, Y. Huang, and I. Cohen, *Pearson Correlation Coefficient*, pp. 1–4. Springer Berlin Heidelberg, 2009.